THE ASTROPHYSICAL JOURNAL, 464:628–640, 1996 June 20

EGRET OBSERVATIONS OF THE NORTH GALACTIC POLE REGION

P. SREEKUMAR,[1,2] D. L. BERTSCH,[1] B. L. DINGUS,[1,2] J. A. ESPOSITO,[1,2] C. E. FICHTEL,[1] J. FIERRO,[3]
R. C. HARTMAN,[1] S. D. HUNTER,[1] G. KANBACH,[4] D. A. KNIFFEN,[5] Y. C. LIN,[3]
H. A. MAYER-HASSELWANDER,[4] J. R. MATTOX,[1,2,6] P. F. MICHELSON,[3]
C. VON MONTIGNY,[1,7] R. MUKHERJEE,[1,2] P. L. NOLAN,[3]
E. SCHNEID,[8] D. J. THOMPSON,[1] AND T. D. WILLIS[3]
Received 1995 March 27; accepted 1996 January 5

ABSTRACT

The EGRET instrument aboard the *Compton Gamma Ray Observatory* (*CGRO*) has carried out the first ever all-sky survey in high-energy gamma rays. Initial analysis of the region near the north Galactic pole showed the presence of several previously undetected point sources, many of which exhibit time variability in the observed emission. A more detailed analysis using all observations during phases I and II of the *CGRO* observing plan shows a total of 21 point sources detected above a 4 σ significance level in the region of the sky with $b > 40°$. Results on source location, possible identification, energy spectrum, and time variability are discussed. Of the 21 sources, 17 are identified as belonging to the blazar class of active galactic nuclei. They include 0917+449, 1127−145, and 1222+216, which are positionally coincident with previous unidentified EGRET sources. The four remaining unidentified sources appear to have no known counterparts. No evidence is found for high-energy gamma-ray emission from M82, M87, or the Coma Cluster. The upper limit from Coma is used to derive a lower limit of 0.4 μG on the intracluster magnetic field.

Subject headings: galaxies: clusters: individual (Coma) — gamma rays: observations — intergalactic medium — surveys

1. INTRODUCTION

The Energetic Gamma-Ray Experiment Telescope (EGRET) on board the *Compton Gamma Ray Observatory* (*CGRO*) covers the high-energy gamma-ray range from approximately 30 MeV to 30 GeV. The all-sky survey by EGRET during the period 1991 April–1993 November (phase I/II) has led to the detection of a number of high-energy gamma-ray sources. This survey provided an opportunity to study in detail high-energy gamma-ray emission from point sources as well as from extended regions of diffuse emission, at higher sensitivity and greater angular resolution than previously possible. Individual observations that are typically two or three weeks in duration are useful in examining the emission from point sources on short timescales, while the sum of many observations provide average fluxes and spectra and improves the detectability of weak, but steady sources. In the case of a time variable source, the analysis using the co-added maps generally show reduced significance compared to the single epoch maps obtained from the viewing period(s) when it was found to be brightest. In this paper we will examine in some detail the north Galactic pole (NGP) region of the sky with Galactic latitude $b > 40°$. Other companion papers by Dingus et al. (1996), Nolan et al. (1996), and Lin et al. (1996) will discuss results from the remaining high-latitude regions of the sky. Similar papers by Kanbach et al. (1996), Kniffen et al. (1996), Bertsch et al. (1996), and Mattox et al. (1996a) will discuss the data along the Galactic plane. Early analysis of the NGP region showed the presence of a few strong sources, including 3C 279, 3C 273, and Mrk 421. Fichtel et al. (1994) presented a summary of results for point sources from the phase I all-sky survey (1991 April to 1992 November). This catalog included nine sources with detection significance greater than 5 σ and five sources at the marginal detection level (between 4 and 5 σ) for Galactic latitudes $b > 40°$. Here we include phase II (1992 November to 1993 September) observations, which added significantly to the phase I exposure. In addition, this analysis includes time history of gamma-ray flux and photon spectra and a more careful determination of position for all sources, including new ones seen only during phase II. Since minimizing the size of the source error box is essential to carry out source identification, efforts were made to reduce the size of the gamma-ray error box. Sections 3, 4, and 5 discuss the spectra and time histories of the detected sources. In most cases, a search for counterparts at other wavelengths showed the presence of known active galactic nuclei (AGNs) within the error box. The nature of the unidentified EGRET sources remains unknown. Additional EGRET observations could reduce the size of their error boxes, making it more feasible to search for candidate counterparts at radio, optical, and X-ray wavelengths. The results from this analysis are included in the second EGRET catalog (Thompson et al. 1995), which provides a summary on the 129 sources seen in the phase I + II observations.

2. OBSERVATIONS AND ANALYSIS

The EGRET instrument and its general capabilities are discussed by Kanbach et al. (1988). The large field of view

[1] NASA/Goddard Space Flight Center, Code 660, Greenbelt MD 20771.
[2] Universities Space Research Association.
[3] W. W. Hansen Experimental Physics Laboratory, Stanford University, Stanford, CA 94305.
[4] Max-Planck-Institut für Extraterrestrische Physik, Postfach 1603, 85740 Garching, Germany.
[5] Hampden-Sydney College, P.O. Box 862, Hampden-Sydney, VA 23943.
[6] Universities of Maryland, College Park, MD 20742.
[7] NAS/NRC Research Associate.
[8] Northrop Grumman Corporation, Mail Stop A01-26, Bethpage, NY 11714.

(~1 sr) is valuable in monitoring multiple gamma-ray sources simultaneously during an observation. This also provides some overlap between different observations, which permits long-term monitoring of time variable sources. The sensitivity is about one-half the on-axis value at 18° from the instrument axis and one-sixth at 30°. Since the photon flux is small at these high energies, the instrumental background must be minimized. EGRET was designed to be free of internal background, and this was verified from prelaunch calibration (Thompson et al. 1993a). The only significant background radiation for point source analysis is the diffuse Galactic and extragalactic radiation. In the region of the sky under study here, the Galactic component is much fainter than the component along the plane of the Galaxy, and so the sensitivity to weak sources is greater.

The co-added exposure map from phase I + II is shown in Figure 1. It shows that the coverage is not uniform over the region under study here. The exposure ranges from 0.09×10^9 cm^2 s to 1.17×10^9 cm^2 s. The added maps use data from individual observing periods within 30° of the pointing direction, within which the exposure and instrument characteristics are best understood. This abrupt cutoff in exposure at 30° causes most of the sharp features in Figure 1. The analysis discussed below was carried out individually for each viewing period (VP) that covered the region of interest here (see Table 1) as well as on the sum of all relevant VPs. Since the Galaxy is itself a strong source of gamma rays arising from the interaction of cosmic rays with the interstellar matter and radiation, we have to use a Galactic diffuse emission model to search for point sources. Along the Galactic plane where the diffuse emission is strongest, we use the detailed model of Hunter et al. (1996) (see also Bertsch et al. 1993), while at high Galactic latitudes, a model based on the total line-of-sight hydrogen (atomic + molecular + ionized) column density is used (Sreekumar et al. 1996). In addition to the Galactic component, a constant isotropic emission of extragalactic origin is also included as background (Thompson & Fichtel 1982; Sreekumar & Kniffen 1996). Flux and upper limits to point sources were determined using a maximum likelihood analysis (Mattox et al. 1996b). This analysis used a background emission model of the form

$$\text{background model} = A \times \text{Galactic diffuse model} + B,$$

where A represents a scale factor to the input Galactic diffuse emission model and B represents an isotropic component, possibly of extragalactic origin. To characterize the existence of a point source at any point in the sky, the coefficients A and B are optimized to maximize likelihood after taking into account the background near the source. The energy-dependent instrument point-spread function (PSF) is used to model the source counts. The detection significance is estimated using the test statistic (TS), which is proportional to the logarithm of the ratio of the likelihoods with and without a source in the model. For the simple case where source position is fixed but the counts are allowed to vary, the TS is distributed as χ^2 with 1 degree of freedom in the null hypothesis, indicating the absence of a source. We can approximately characterize the source detection significance in sigmas by the square root of TS. A more detailed account on the likelihood method used to analyze EGRET point sources is available in Mattox et al. (1996b). The analysis proceeds as follows. An initial list of point source locations are derived from the $E > 100$ MeV integral map, which roughly provides the optimal combination of source counts and angular resolution (FWHM = 5° at 100 MeV). Starting from maps of counts and exposure (generally binned at 0°.5 × 0°.5), the likelihood TS is determined at every pixel in the map with exposure greater than some

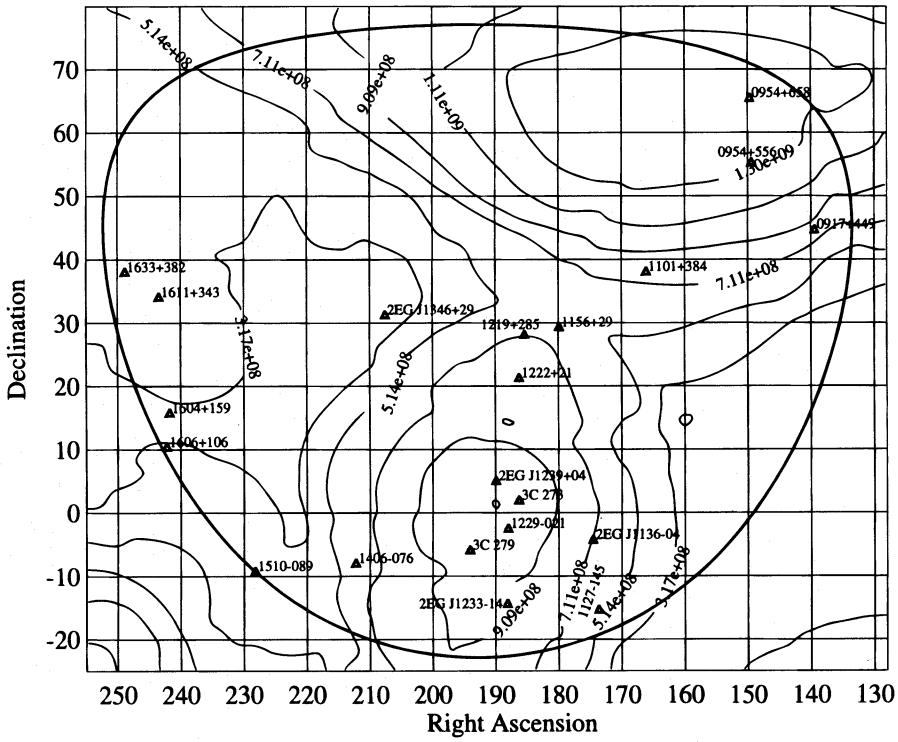

FIG. 1.—EGRET exposure (cm^2 s) contours near the north Galactic pole region. The region of the sky examined in this paper is shown by the thick solid line ($b > 40°$). Detected gamma-ray sources are also indicated. Source flux and spectral index are given in Tables 2 and 3.

TABLE 1

VIEWING PERIODS IN PHASES I AND II THAT COVER REGIONS WITH LATITUDE >40°

VP	Start	Stop	l	b
0.6	1991 May 07 16:35	1991 May 10 19:39	150°.00	53°.00
3.0	1991 Jun 15 23:24	1991 Jun 28 19:30	299.76	65.46
4.0	1991 Jun 28 20:43	1991 Jul 12 17:56	156.18	72.08
9.2	1991 Sep 12 14:34	1991 Sep 19 12:52	59.67	40.28
11.0	1991 Oct 03 14:19	1991 Oct 17 13:57	294.25	63.67
12.0	1991 Oct 17 15:22	1991 Oct 31 14:52	310.71	22.21
16.0	1991 Dec 12 18:00	1991 Dec 27 16:01	0.00	20.28
18.0	1992 Jan 10 18:21	1992 Jan 23 13:38	137.47	40.49
22.0	1992 Mar 05 16:45	1992 Mar 19 12:00	112.47	44.46
24.0	1992 Apr 02 15:05	1992 Apr 09 12:15	9.53	57.15
24.5	1992 Apr 09 15:15	1992 Apr 16 10:43	9.53	57.15
25.0	1992 Apr 16 15:19	1992 Apr 23 10:41	6.84	48.09
31.0	1992 Jun 11 16:25	1992 Jun 25 12:08	163.09	11.92
32.0	1992 Jun 25 14:46	1992 Jul 02 13:23	284.20	22.89
33.0	1992 Jul 02 16.08	1992 Jul 16 14:40	252.41	30.66
40.0	1992 Sep 17 16:56	1992 Oct 08 13:15	195.90	44.71
201.0	1992 Nov 17 17:17	1992 Nov 24 16:03	66.79	39.28
202.0	1992 Nov 24 17:50	1992 Dec 01 15:08	70.85	40.50
204.0	1992 Dec 22 14:52	1992 Dec 29 13:57	294.70	61.88
205.0	1992 Dec 29 18:14	1993 Jan 05 12:38	294.46	61.58
206.0.....	1993 Jan 05 17:13	1993 Jan 12 13:00	294.70	61.88
207.0	1993 Jan 12 16:13	1993 Feb 02 12:46	314.06	31.51
208.0	1993 Feb 02 16:22	1993 Feb 09 15:05	307.39	20.75
212.0	1993 Mar 09 16:51	1993 Mar 23 16:23	83.74	11.67
215.0	1993 Apr 01 17:48	1993 Apr 06 19:13	311.66	22.89
216.0	1993 Apr 06 21:10	1993 Apr 12 11:24	140.75	38.11
217.0	1993 Apr 12 13:50	1993 Apr 20 12:27	311.66	22.89
218.0	1993 Apr 20 15:56	1993 May 03 21:04	151.41	71.26
219.0	1993 May 05 16:06	1993 May 06 21:40	350.10	15.86
222.0	1993 May 24 17:15	1993 May 31 12:13	157.79	70.63
227.0	1993 Jun 29 15:00	1993 Jul 13 12:37	148.11	41.22
228.0	1993 Jul 13 14:07	1993 Jul 27 11:35	149.86	42.69

threshold value. Regions of high TS indicate potential point sources. The strongest sources are modeled first. A more detailed search is carried out for weaker sources after including the strong ones into the background model. The final source counts are derived self-consistently by iteration. This analysis uses binned data and therefore does not exploit the full directional information from each photon, the higher energy photons having smaller uncertainty in the arrival direction. However, significantly improved source positions are derived by carrying out the likelihood analysis in four independent energy ranges (30–100; 100–300; 300–1000, and >1000 MeV) using the appropriate energy-dependent PSF and then summing the resulting maps in log likelihood space. The FWHM at 30, 100, 300, and 1000 MeV are 14°.5, 5°.6, 3°, and 1°.2, respectively. Thus, the final source position estimate takes some advantage of the significantly tighter PSF at high energies. It is important to note that using binned maps with photons above 100 MeV, the limited angular resolution of EGRET, results in typical error circles as large as 0°.5 or more in radius, except for the strongest sources. This makes unique source identification difficult, since these error boxes often contain several astronomical objects, including stars, radio, *IRAS* or X-ray sources, and normal galaxies. Stars, *IRAS* sources, and normal galaxies are, in general, ignored, since their sky densities lead to one or more chance coincidences in a typical EGRET error box. So far, only one normal galaxy (LMC) has been seen in gamma rays above 100 MeV, and no detectable emission is seen from other nearby candidate galaxies (Sreekumar et al. 1992, 1994). No detectable emission is seen from even the nearby rich Coma Cluster. So, in addition, we do not consider galaxy clusters as likely counterparts. In this paper we follow the approach described by Hartman et al. (1993) to carry out source identifications. Source spectra are determined using 10 sub-energy intervals ranging from 30 MeV to 10 GeV. The power-law fits are determined using a χ^2 minimization method after forward folding though the EGRET response function. The 1 σ error in the spectral index is obtained using the size of the parameter space defined by $\chi^2 < \chi^2 + 1.0$. This is appropriate in the analysis presented here, since the integral fluxes stated in Tables 2–4 are independently derived from the $E > 100$ MeV maps and not from integrating the given spectral fits (see Dingus et al. 1996 for details).

Section 3 discusses the results on the detected AGNs and § 4 on the unidentified source. The region of the sky beyond 40° latitude also contains other interesting sources, such as the Coma Cluster and galaxies such as M87 and M82. Section 5 discusses upper limits on the gamma-ray emission from these sources and their implications.

3. BLAZARS

Observations and results from a few of the sources in our region of interest have been previously reported: 3C 273 (von Montigny et al. 1993), 3C 279 (Hartman et al. 1992; Kniffen et al. 1993), Mrk 421 (Lin et al. 1992), 1633+382 (Mattox et al. 1993), 1510−089 (Thompson et al. 1993b), and 0954+658 (Mukherjee et al. 1995). For time variability plots on 3C 279, 3C 273, and 1633+382, see Figure 4 in von Montigny et al. (1995). Multiwavelength spectra for most of the identified sources in this region are also included in von Montigny et al. (1995) together with an extensive discussion on the implication of EGRET detections on AGN models.

TABLE 2

AGNs Detected at High Significance Near the North Galactic Pole

Source	R.A.[a]	decl.[a]	Δ[b]	δr[c]	Counts[d]	Flux[e]	γ[f]	VP[g]	z[h]
0917+449.....	139.43	44.80	35′	48′	101	1.19 ± 0.23	1.98 ± 0.25	p12	2.180
0954+556.....	149.20	55.03	22	48	82	0.61 ± 0.17	1.63 ± 0.23	p12	0.901
0954+658.....	149.30	65.70	13	30	98	0.64 ± 0.17	2.05 ± 0.23	p12	0.368
1101+384.....	166.16	38.03	11	30	118	1.43 ± 0.22	1.58 ± 0.22	p12	0.031
1127−145.....	173.62	−15.23	25	45	36	9.27 ± 2.29	2.15 ± 0.36	206	1.187
1156+295.....	179.64	29.31	14	63	26	19.22 ± 4.78	2.21 ± 0.52	206	0.729
			...	...	...	<1.65	...	3	
			...	...	...	<0.75	...	4	
			...	...	...	<1.56	...	11	
			...	...	...	<5.03	...	204	
			...	...	...	6.44 ± 3.32	...	205	
			...	...	...	<2.60	...	218	
			...	...	...	<3.17	...	222	
1219+285.....	185.58	28.44	16	24	42	0.58 ± 0.18	1.27 ± 0.39	p12	0.102
1222+216.....	186.50	22.58	74	74	159	2.35 ± 0.59	2.58 ± 0.15	p12	0.435
						2.34 ± 0.44	2.50 ± 0.21	3 + 4	
			...	...	...	<1.22	...	11	
			...	...	...	8.31 ± 1.97	1.85 ± 0.37	204	
			...	...	...	3.27 ± 1.62	...	205	
			...	...	...	<2.85	...	206	
			...	...	...	2.42 ± 1.15	...	218	
			...	...	...	<4.83	...	222	
1226+023.....	186.98	2.15	37	42	178	1.63 ± 0.27	2.52 ± 0.27	p12	0.158
1229−021.....	187.89	−2.21	13	75	109	1.02 ± 0.24	2.92 ± 0.44	p12	1.0448
1253−055.....	194.05	−5.80	1	9	1384	13.46 ± 0.49	1.96 ± 0.03	p12	0.538
			...	...	...	28.68 ± 1.09	1.89 ± 0.06	3	
			...	...	...	9.25 ± 0.77	2.07 ± 0.10	11	
			...	...	...	13.53 ± 4.98	...	24	
			...	...	...	<4.85	...	24.5	
			...	...	...	<11.40	...	25	
			...	...	...	<2.91	...	204	
			...	...	...	<3.16	...	205	
			...	...	...	1.44 ± 0.96	...	206	
			...	...	...	<2.96	...	207	
1406−076.....	212.45	−7.75	15	27	270	4.57 ± 0.44	2.04 ± 0.11	p12	1.494
			...	...	...	<0.99	...	3	
			...	...	...	<2.44	...	11	
			...	...	...	<4.51	...	24	
			...	...	...	8.70 ± 2.27	2.08 ± 0.36	24.5	
			...	...	...	3.56 ± 1.55	...	25	
			...	...	...	7.64 ± 1.94	...	204	
			...	...	...	14.45 ± 2.64	2.03 ± 0.12	205	
			...	...	...	10.44 ± 2.59	...	206	
			...	...	...	12.16 ± 1.56	...	207	
1510−089.....	227.95	−9.31	20	90	81	2.30 ± 0.57	2.51 ± 0.36	p12	0.361
1606+106.....	242.16	10.90	25	51	130	3.81 ± 0.61	2.54 ± 0.23	p12	1.24
			...	...	...	<2.98	...	9.2	
			...	...	...	5.75 ± 1.26	...	16	
			...	...	...	2.76 ± 0.73	...	24	
1604+159.....	241.28	15.36	42	75	27	3.98 ± 1.22	1.99 ± 0.50	25	...
1611+343.....	243.63	34.42	16	24	71	1.75 ± 0.39	1.99 ± 0.24	p12	1.404
			...	...	...	<1.20	...	9.2	
			...	...	...	<1.28	...	24	
			...	...	...	4.18 ± 1.14	...	201	
			...	...	...	5.38 ± 1.28	...	202	
1633+382.....	249.01	38.31	14	18	323	7.58 ± 0.63	2.06 ± 0.08	p12	1.810
			...	...	...	10.51 ± 0.94	...	9.2	
			...	...	...	4.22 ± 1.08	...	201	
			...	...	...	3.24 ± 1.08	...	202	

[a] Measured source position (right ascension and declination) in degrees.
[b] Difference in arcminutes between measured source position and known radio position.
[c] Radius of 95% confidence position error circle in arcminutes.
[d] Measured source counts above 100 MeV.
[e] Flux or 2 σ upper limit above 100 MeV in units of 10^{-7} photons cm^{-2} s^{-1}.
[f] Photon spectral index. Uncertainties are derived from $\chi^2_{\rm min} + 1.0$.
[g] Viewing period (p12 = phase I + II).
[h] Redshift.

TABLE 3

UNIDENTIFIED EGRET SOURCES NEAR THE NORTH GALACTIC POLE

Source ID[a]	R.A.[b]	decl.[b]	δr[c]	Counts[d]	Flux[e]	γ[f]
2EG J1136−04[g]	174.23	−4.24	46[h]	36	1.67 ± 0.51	...
2EG J1233−14	188.26	−14.13	96	90	0.93 ± 0.25	1.96 ± 0.25
2EG J1239+04	189.82	4.69	53	171	1.60 ± 0.28	2.89 ± 0.25
2EG J1346+29[i]	206.70	29.70	56	26	2.14 ± 0.68	...

[a] Name in R.A. and decl. (J2000 epoch): format hhmm ± dd.
[b] Measured source position (right ascension and declination).
[c] Radius of 95% confidence position error circle in arcminutes.
[d] Measured source counts above 100 MeV.
[e] Flux (>100 MeV) averaged over phases I and II (unless otherwise noted) in units of 10^{-7} photons cm^{-2} s^{-1}.
[f] Photon spectral index. Uncertainties are derived from $\chi^2_{\rm min} + 1.0$.
[g] Extended source. Position error corresponds to 1 σ confidence contour.
[h] Source parameters derived from VP 3.0.
[i] Source parameters derived from VP 4.0.

Here we will summarize the results from a more complete and thorough analysis of phase I + II data. A total of 21 sources were seen at a significance larger than 4 σ in the EGRET data from phases I and II (Fig. 1). Of these, 17 have been identified as AGNs, while the remaining four show no likely counterparts at other wavelengths. New results on a few selected sources ordered by right ascension are separately described below. Table 2 summarizes the results on the detected AGNs, and Table 4 gives the observed fluxes in the four broad energy intervals.

3.1. *Results*

3.1.1. *0917+449*

The previously unidentified gamma-ray source GRO J0916 + 43 (Fichtel et al. 1994) has now been identified as the flat spectrum radio quasar 0917 + 449. This source has a radio spectral index (α) of −0.08, a flux of 1 Jy at 4.85 GHz, and is 35′ away from the best measured position of the source (95% error circle = 48′). Unlike most other EGRET-detected AGNs, the gamma-ray emission from 0917+449 appears steady during the different EGRET observations in phases I and II. The photon spectrum averaged over phases I and II is

$$dN/dE = (1.56 \pm 0.29) \times 10^{-10}(E/285)^{-1.98\pm0.25}$$

photons cm^{-2} s^{-1} MeV^{-1}.

3.1.2. *0954+55*

The object 0954+556 (4C 55.19) is a strong radio source (2.17 Jy at 5 GHz; Impey & Tapia 1990) that exhibits high optical polarization (~9%). Radio measurements at 2.7 and 4.9 GHz indicate a flat radio spectrum ($\alpha = -0.22$). The object 0954+556 is detected as a weak gamma ray source

TABLE 4

INTEGRAL FLUXES IN FOUR BROAD ENERGY BANDS FOR ALL DETECTED SOURCES

Source	F_{30-100}	$F_{100-300}$	$F_{300-1000}$	$F_{>1000}$
0917+449	19.02 ± 13.42	5.38 ± 2.02	4.45 ± 0.98	<4.0
0954+556	<19.65	4.72 ± 1.64	1.19 ± 0.57	0.94 ± 0.38
0954+658	<20.24	4.08 ± 1.73	1.70 ± 0.58	0.61 ± 0.31
1101+384	<30.50	7.17 ± 2.04	2.87 ± 0.84	2.59 ± 0.73
1127−145[a]	<227.7	54.24 ± 12.01	18.27 ± 6.07	<4.3
1156+295[b]	<508.96	139.26 ± 45.36	30.84 ± 16.57	43.35 ± 23.81
1219+285	<26.80	2.63 ± 2.08	1.50 ± 0.73	1.61 ± 0.63
1222+216	98.82 ± 17.61	17.47 ± 2.82	4.77 ± 1.12	<0.5
1226+023	43.24 ± 17.09	9.81 ± 2.44	4.65 ± 0.99	0.25 ± 0.22
1229−021	37.73 ± 17.24	12.05 ± 2.51	1.08 ± 0.66	<0.7
1253−055	276.30 ± 20.57	79.74 ± 4.00	37.96 ± 2.20	11.93 ± 1.36
1406−076	67.46 ± 20.88	24.26 ± 3.58	12.03 ± 1.94	3.63 ± 1.09
1510−089	<79.67	21.87 ± 5.16	<4.40	<2.5
1604+159[c]	<114.75	22.63 ± 10.14	10.45 ± 5.10	<9.9
1606+106	76.36 ± 29.69	29.95 ± 5.25	4.19 ± 1.78	<2.5
1611+343	<64.33	10.89 ± 3.85	4.63 ± 1.45	1.90 ± 0.88
1633+382	162.35 ± 30.76	44.92 ± 5.26	19.20 ± 2.61	5.49 ± 1.49
2EG J1136−04[d]	78.08 ± 32.67	12.97 ± 4.81	<4.6	<5.2
2EG J1233−14	24.91 ± 16.99	6.69 ± 2.42	1.31 ± 0.80	1.47 ± 0.58
2EG J1239+04	99.50 ± 18.27	13.29 ± 2.55	0.98 ± 0.71	1.02 ± 0.48
2EG J1346+29[e]	121.78 ± 45.65	11.29 ± 6.40	<5.3	<2.74

NOTE.—Photon flux corresponds to the average value derived for the summed data (unless otherwise noted) in units of 10^{-8} photons cm^{-2} s^{-1}. The 1 σ errors are statistical and upper limits are 95% confidence. Energy ranges are expressed in units of MeV.
[a] Results from VPs 205.0 and 206.0.
[b] Results from VP 206.0.
[c] Results from VP 25.0.
[d] Results from VP 3.0.
[e] Results from VP 4.0.

(4.2 σ) in the phase I + II data. The flux/upper limit from the individual observations do not show clear evidence for time variability. The average photon spectrum is

$$dN/dE = (1.91 \pm 0.45) \times 10^{-11}(E/606)^{-1.98\pm0.28}$$

photons cm^{-2} s^{-1} MeV^{-1}

3.1.3. *1101+384 (Mrk 421)*

Mrk 421 is the nearest BL Lac object, at a redshift of $z = 0.0308$. Results from phase I and phase II are discussed by Lin et al. (1992) and Lin et al. (1993), respectively. Our analysis indicates no significant time variability in gamma rays, unlike the rapid variability observed at radio, infrared, and optical wavelengths and unlike gamma-ray observations of other blazars, such as 3C 279 or PKS 1406−076. Our analysis (phases I and II) indicates a single power-law spectrum with an index of 1.58 ± 0.22:

$$dN/dE = (3.91 \pm 0.70) \times 10^{-11}(E/571)^{-1.58\pm0.22}$$

photons cm^{-2} s^{-1} MeV^{-1} .

There is marginal evidence for a spectral break from MeV to TeV energies (Schubnell et al. 1993; $\gamma = 2.25 \pm 0.3$). The EGRET detection of Mrk 421 is especially interesting since it is one of the only two blazars detected at TeV energies (Punch et al. 1992; Mohanty et al. 1993).

3.1.4. *1156+295*

The object 1156+295 is an optically violent variable (OVV) quasar with a flat radio spectrum ($\alpha = -0.1$), high polarization, and an estimated redshift of $z = 0.729$. The only strong detection of 1156+295 (4C 29.25) was during a one week observation in VP 206 (6.8 σ), when the source was about 30° away from the EGRET z-axis. One week earlier (VP 205), there was only a 2.6 σ evidence for this source and the deduced flux of $(6.44 \pm 3.33) \times 10^{-7}$ photons cm^{-2} s^{-1} was about one-third that found in VP 206 (Fig. 2). The flux during the outburst is about 50% of the 3C 279 flux during its outburst (VP 3). In Figure 3 the source flux (>100 MeV) in VP 206 is shown over a 1 day time interval. The outburst appears to have lasted only over a short timescale of a few days. This is similar to the flare seen in 3C 279 during VP 3. The observed average power-law spectrum in VP 206 is

$$dN/dE = (2.17 \pm 0.77) \times 10^{-9}(E/242)^{-2.21\pm0.52}$$

photons cm^{-2} s^{-1} MeV^{-1} .

3.1.5. *1219+285*

The source 1219+285 is a relatively nearby BL Lac object ($z = 0.102$), and it shows the hardest measured spectrum (~ 1.27) among the current EGRET AGN detections. The source is barely visible below 300 MeV and is strongly detected above 1 GeV (>5 σ). The data does not show evidence for time variability. The average photon spectrum is

$$dN/dE = (1.14 \pm 0.34) \times 10^{-11}(E/882)^{-1.27\pm0.39}$$

photons cm^{-2} s^{-1} MeV^{-1} .

On 1992 February 24, Massaro, Nesci, & Perola (1992) reported this source at its brightest in optical wavelengths since 1972. However, no EGRET observations are available during the same time frame to address the existence of a correlated outburst at gamma-ray energies.

3.1.6. *1222+023 (3C 273)*

The object 3C 273 was the first extragalactic source detected in high-energy gamma rays (Swanenburg et al. 1978; Hermsen et al. 1981). At a $z = 0.158$, 3C 273 is one of the best studied quasars at all wavelengths, and its time variability has led to numerous observing campaigns at different wavelengths to examine the nature of this object (Ulrich, Courvoisier, & Wamsteker 1993; Courvoisier et al. 1987). Observations during phases I and II indicates 3C 273 has decreased in strength from the initial phase I observations (VPs 3 and 11; von Montigny et al. 1993). The data are not sufficient to examine short timescale variability. The gamma-ray spectrum is characterized by a rather steep power law with an index of 2.52 ± 0.18 and a flux of $(1.67 \pm 0.27) \times 10^{-7}$ photons cm^{-2} s^{-1} for $E > 100$ MeV. The mean differential photon spectrum averaged over all phase I and II observations is

$$dN/dE = (4.00 \pm 0.64) \times 10^{-10}(E/191)^{-2.52\pm0.18}$$

photons cm^{-2} s^{-1} MeV^{-1} .

This source was seen by *COS B* in a relatively high gamma-ray state with a flux above 100 MeV of 6.0×10^{-7} photons cm^{-2} s^{-1} (Swanenburg et al. 1978; Bignami et al. 1981). It has never been observed at that high level of activity during the first 2.5 years of EGRET observations.

3.1.7. *1222+216*

Even though the first EGRET catalog (Fichtel et al. 1994) reported the presence of the unidentified gamma-ray source GRO J1222+22, it was later identified with the flat spectrum radio quasar 1222+216. It was detected as a 6.2 σ source in VP 204. Figure 2 shows the source to be time variable above 100 MeV. No short timescale variability is observed in the data. We examined the source spectrum separately (Fig. 4) when the source was detected in the *high* state (VP 204) and in the *low* state (VP 3 + 4). VP 204 observations showed a single power-law photon spectrum with an index of 1.85 ± 0.37. During VP 3 + 4 the power law has an index of 2.50 ± 0.21. This indication for hardening of the spectrum during an outburst appears consistent with a similar trend seen in 0528+134 (Mukherjee et al. 1996). The separate spectral fits are given below.

VP 3 and 4:

$$dN/dE = (8.62 \pm 1.39) \times 10^{-10}(E/172)^{-2.50\pm0.21}$$

photons cm^{-2} s^{-1} MeV^{-1} .

VP 204:

$$dN/dE = (1.45 \pm 0.38) \times 10^{-9}(E/213)^{-1.85\pm0.37}$$

photons cm^{-2} s^{-1} MeV^{-1} .

3.1.8. *1253−055 (3C 279)*

Soon after the launch of *CGRO*, EGRET observed the Virgo region and detected a very bright source not far from the only AGN known previously to emit in gamma rays, namely, 3C 273. This source was identified to be the gamma-ray counterpart of 3C 279 (Hartman et al. 1992). Kniffen et al. (1993) have discussed results from the first detection of 3C 279, during which the gamma-ray emission increased over a few days to about 4 times the initial observed flux followed by a rapid decrease over a two day time interval. Later EGRET observations have not shown a

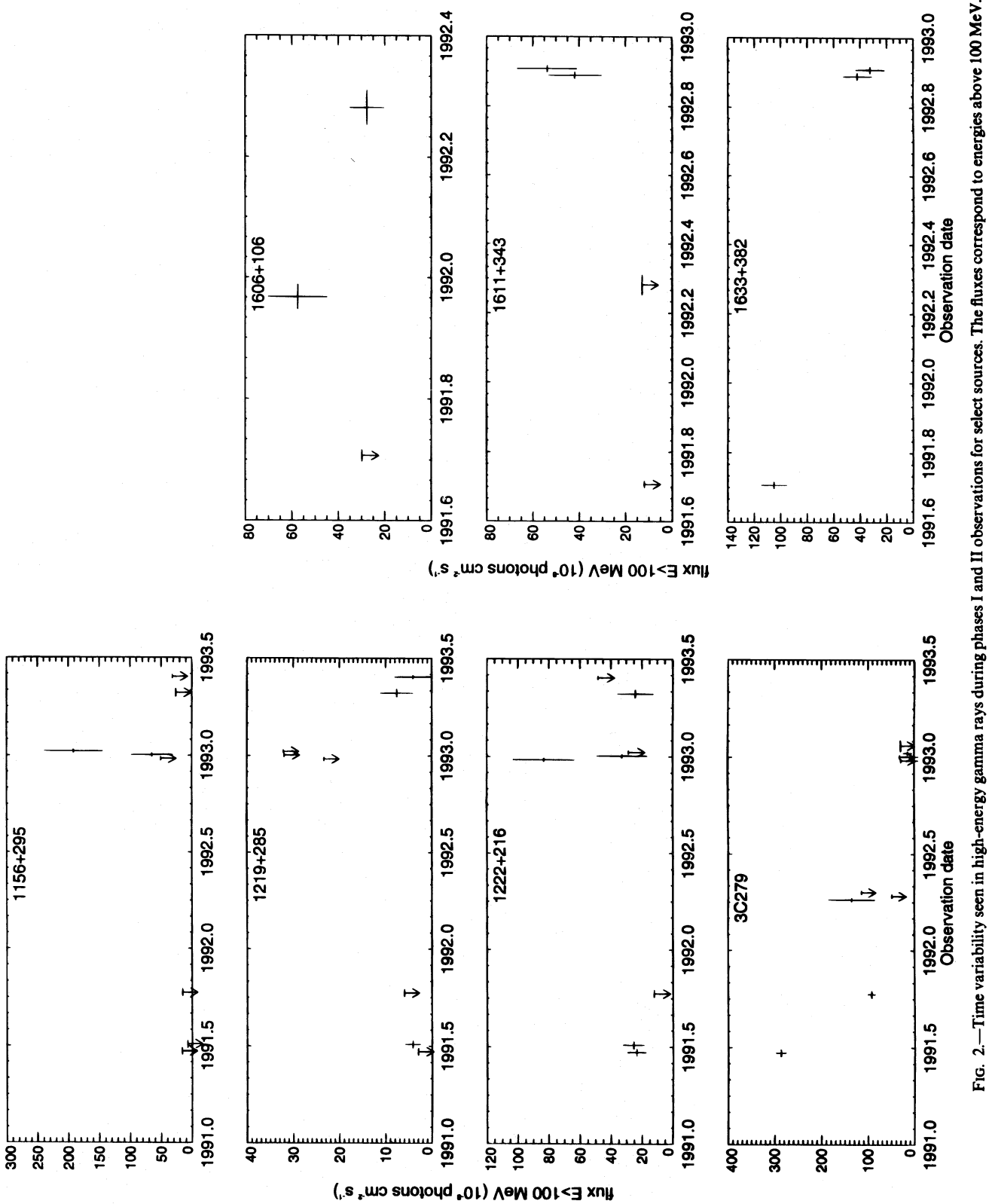

FIG. 2.—Time variability seen in high-energy gamma rays during phases I and II observations for select sources. The fluxes correspond to energies above 100 MeV.

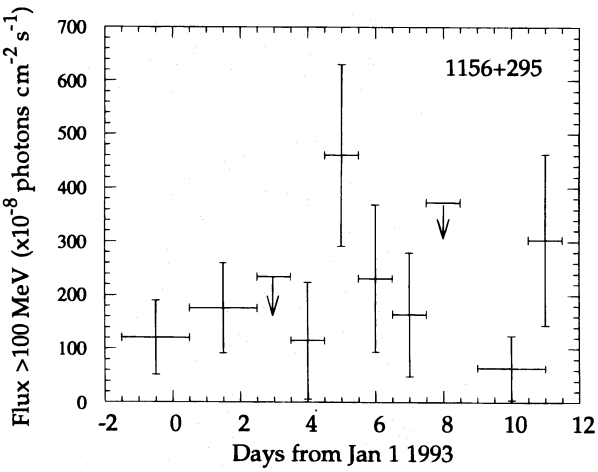

FIG. 3.—Short timescale variability seen in 1156+295 during the only observations when the source was clearly detected (VP 206).

similar large flare in gamma rays. Figure 2 shows the variability in the $E > 100$ MeV flux from 3C 279 over a timescale of many years. The observations in phase II (VPs 204, 205, 206, 207) show the gamma ray flux has decreased even below that seen during VP 11. The average photon spectrum from the combined data from phases I and II is described best by a power law as

$$dN/dE = (1.73 \pm 0.05) \times 10^{-9}(E/249)^{-1.96\pm0.03}$$

photons cm^{-2} s^{-1} MeV^{-1},

consistent with previously published results. No significant change in the slope of the power-law spectrum was observed between the outburst in VP 3 and the weaker detection in VP 11 (Kniffen et al. 1993). Because of the reduced level of gamma-ray emission since the initial outburst, no evidence on the short timescale variability is available from subsequent observations.

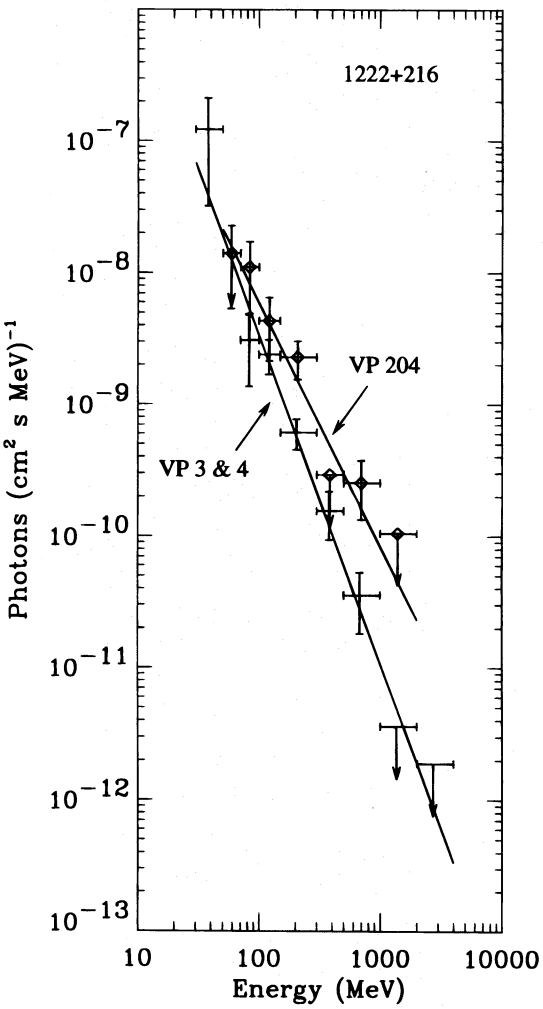

FIG. 4.—Variability seen in 1222+216 gamma-ray spectrum during viewing periods 3 + 4 and 204. The spectrum shows a tendency to be harder when the source is brighter (VP 204).

3.1.9. *1406−076*

PKS 1406−076 is a low-polarization quasar at a redshift of $z = 1.494$. It is a flat spectrum radio source ($\alpha = 0.25$) with about a 1 Jy radio flux at 5 GHz. The tentative detection of this source was first reported by Dingus et al. (1993), when it was seen to be bright gamma-ray source during VP 207. The time history of gamma-ray emission from this source is shown in Figure 5. During 1992 December and 1993 January when 1406−076 was observed to be in a high state, it was observed almost continuously by EGRET for over a month. However, no statistically significant evidence exists for variability on short timescales (2 days or less), as was seen in 3C 279. Data from phase II (VP 205 + 206 + 207) when the source was brightest, gives a power-law photon spectrum of index 2.02 ± 0.12. This is consistent with the value derived when the source was detected in a *low* state (VP 24 + 24.5 + 25) of 2.08 ± 0.36. The average phase I + II spectrum is

$$dN/dE = (4.85 \pm 0.51) \times 10^{-10}(E/261)^{-2.04\pm0.11}$$

photons cm^{-2} s^{-1} MeV^{-1}.

3.1.10. *1510−089*

PKS 1510−089 is a bright radio source (3 Jy at 5 GHz; Impey & Tapia 1990) and is classified as a highly polarized quasar (HPQ). It is considered a *possible* superluminal radio source. Thompson et al. (1993b) discussed the initial EGRET results on this source. This is a weak gamma-ray source, and the observations do not indicate variability at energies greater than 100 MeV. The average spectrum is described by

$$dN/dE = (9.45 \pm 2.40) \times 10^{-10}(E/160)^{-2.51\pm0.36}$$

photons cm^{-2} s^{-1} MeV^{-1}.

3.1.11. *1606+106*

PKS 1606+106 is strongly detected in VP 16 (6 σ). Observations during VP 24, 24.5 and 25 indicate that the flux above 100 MeV has decreased by about 50% (Fig. 2). No additional exposure was obtained during phase II. The average gamma-ray spectrum is

$$dN/dE = (1.64 \pm 0.24) \times 10^{-9}(E/154)^{-2.54\pm0.23}$$

photons cm^{-2} s^{-1} MeV^{-1}.

3.1.12. *1604+159*

The BL Lac object 1604+159 has no measured redshift. It was detected in gamma rays only once (VP 25) as a 4.9 σ source. The phase I and II data do not clearly establish variability at gamma-ray energies. The average gamma-ray

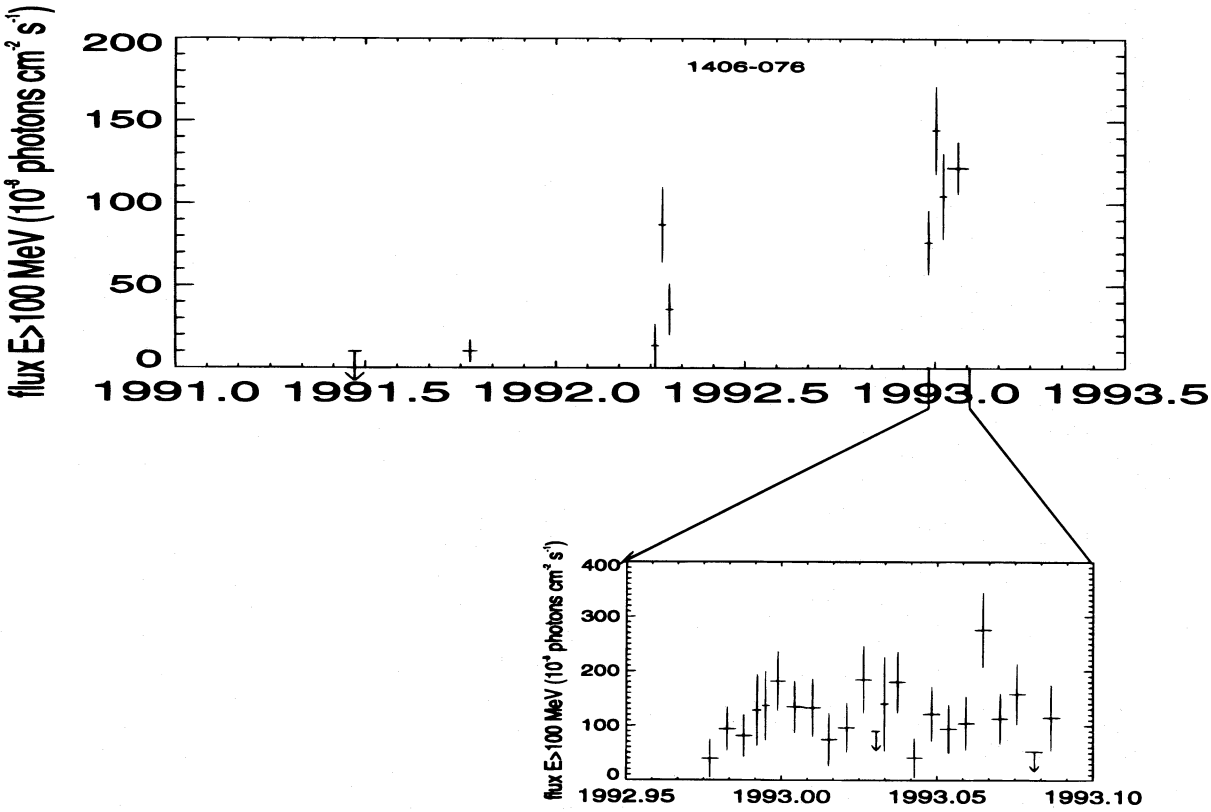

FIG. 5.—Time variability of gamma-ray emission from 1406−076 at energies above 100 MeV

spectrum is

$$dN/dE = (2.40 \pm 0.86) \times 10^{-10}(E/379)^{-1.99\pm0.50}$$

photons cm^{-2} s^{-1} MeV^{-1}.

3.1.13. *1611+343*

The source 1611+343 was detected in gamma rays only during VPs 201 and 202. A previous favorable observation by EGRET showed no detectable emission from this source. Figure 2 shows the change in the observed flux during this time period. The upper limits obtained for the early observations indicate that this source is also variable in gamma rays over a timescale of months. There is no indication of variability on shorter timescales within VPs 201 and 202. The average gamma-ray photon spectrum over VPs 201 and 202 is

$$dN/dE = (5.55 \pm 1.06) \times 10^{-10}(E/272)^{-1.99\pm0.24}$$

photons cm^{-2} s^{-1} MeV^{-1}.

3.1.14. *1633+382*

EGRET detection of 1633+382 reported by Mattox et al. (1993) were based on seven days of observations in 1991 September. The gamma-ray flux varied by a factor of 3 during the days. Since then an additional two weeks of observations during phase II indicate that the flux above 100 MeV has dropped by about a factor of 3 below the mean flux reported by Mattox et al. (1993). Unlike the phase I observation, no short timescale variability is seen within the phase II data. Figure 2 shows the measured flux above 100 MeV during the three VPs 9.5, 201 and 202. The power law spectrum from VP 9.2 (when the source was bright) is superimposed on the combined (VPs 201 and 202) spectra in Figure 6. Even though it is not statistically significant, there appears to be a tendency for spectral hardening when the source is in an outburst. The respective power-law fits are

VP 9.2:

$$dN/dE = (1.48 \pm 0.13) \times 10^{-9}(E/256)^{-2.03\pm0.09}$$

photons cm^{-2} s^{-1} MeV^{-1},

VP 201 and 202:

$$dN/dE = (5.63 \pm 1.15) \times 10^{-10}(E/243)^{-2.20\pm0.25}$$

photons cm^{-2} s^{-1} MeV^{-1}.

3.2. *Discussion*

The observational results presented above indicate that a subset of the AGN family of sources (blazars) dominate the extragalactic point sources seen by EGRET. The bulk of the power emitted by these blazars (particularly the non-BL Lacs) resides in photons at MeV and GeV energies, as is evident from the νF_ν plots in von Montigny et al. (1995). For the detections discussed here, a power-law fit to the observed gamma-ray spectrum ranges from 1.3 to 2.9. Most of the gamma-ray bright blazars show time variability ranging from 2 days to over a period of many months or years (see Table 3 in von Montigny et al. 1995). In most cases, the low count rate does not permit examination of variability at smaller time intervals. On a simplistic approach, this can be used to place a minimum on the size of the region from which the gamma-ray emission originates. However, most models require relativistic beaming in the jet, and the minimum size depends on the bulk Lorentz factor assumed in the model.

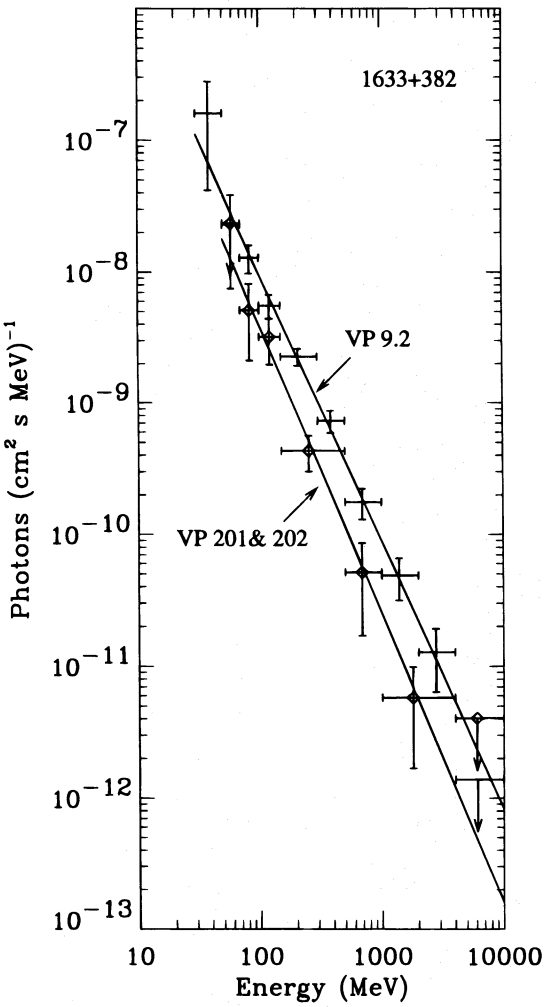

FIG. 6.—Variability seen in 1633+382 gamma-ray spectrum during viewing periods 9.2 (*high*) and (201+202) (*low*).

Sources that show outbursts in gamma rays and are also detectable in their quiet phase can be used to address correlation of spectral variability with intensity. This can be studied in 3C 279, 1633+382, 1406−076, and 1222+216. The source 1222+216 shows marginal evidence for spectral hardening during outbursts. Agarwal, Singh, & Riegler (1987) have shown a similar trend in certain BL Lac objects at X-ray energies. Sambruna et al. (1994) also reported similar spectral hardening with increasing intensity in X-ray–selected BL Lac objects. The objects 3C 279, 1406−076 and 1633+382 show no statistically significant correlation of power-law spectra with source intensity. However, all three sources show a tendency similar to that in 1222+216, for the spectrum to harden with increasing source intensity. Examining additional data acquired since the end of phase II may provide new evidence for spectral evolution during outbursts.

The general approach to explain the high-energy gamma-ray emission from blazar-type AGNs assumes these are generally flat spectrum radio bright sources, characterized by Doppler-boosted jets of relativistic particles directed toward us (Blandford & Rees 1978; Blandford & Königl 1979; Maraschi, Ghisellini, & Celotti 1992; Dermer, Schlickeiser, & Mastichiadis 1992; Sikora, Begelman, & Rees 1994). At low energies, the radiation is understood to arise primarily from synchrotron emission by relativistic electrons, while the high-energy emission is most probably via Compton upscattering of soft photons by a relativistic particle flow in a jet. A primary difference between many models used to explain the high-energy emission is in the source of the soft photon population. Based on the original idea of Ginzburg & Syrovatski (1969), the synchrotron self-Compton (SSC) models assume that the soft photons created by the synchrotron process are themselves energerized to higher energies by the same population of relativistic electrons that gave rise to the photons in the first place. Bloom & Marscher (1992) showed that the standard SSC model is not successful in explaining strong gamma-ray emission from blazars. Another approach that appears more viable (Melia & Königl 1989); Dermer et al. 1992; Sikora et al. 1994) assumes the soft photons used as seed for inverse Compton scattering arise not from the jet but from the accretion disk, possibly reprocessed and scattered by material above the disk. The details on delayed or simultaneous emission at various frequencies predicted by each model depends on specific model parameters, including source geometry. It is clear that simultaneous radio, infrared, optical, and UV observations are essential in constraining the various jet models being proposed. A more complete and detailed summary of blazar models that explains the high-energy gamma-ray emission can be found in von Montigny et al. (1995).

4. UNIDENTIFIED SOURCES

In addition to gamma-ray sources positionally identified with AGNs, EGRET observations also show the presence of many point sources that appear to have no *likely* counterparts at any other wavelengths. Considering the fact that EGRET detections of many high-latitude sources appear to be coincident with flat spectrum, bright radio sources, a similar search was made using the NASA Extraterrestrial Database (NED), and it yielded no such candidate above a radio flux threshold of 0.3 Jy at 4.85 GHz in the EGRET error box for these sources. Radio catalogs do not always give the full range of observed radio fluxes at any frequency. So it is conceivable that a likely flat spectrum radio counterpart, though currently listed with flux below our selection threshold, has, in the long run, phases of higher radio flux and therefore must be considered seriously as an identification. Another possibility is that these are nearby (due to the large observed scale height of these sources) pulsars (since pulsars are the only other gamma-ray point sources seen by EGRET outside AGNs) that either have no observable radio emission (e.g., Geminga) or have missed detection because of either an unfavorable radio beam geometry or intensity. Unfortunately, gamma-ray sources cannot be searched for periodicity unless they are very bright and have a small location error box (~arcmin). It is also possible that they represent a new class of gamma-ray bright sources in the universe. To further assist in the resolution of this issue, we report here new results on the spectral and temporal properties and more refined positions of these unidentified sources. For example, time variability in the gamma-ray emission is a characteristic more typical of AGNs than gamma-ray pulsars seen by EGRET. New multiwavelength observations can also assist in determining the nature of the unidentified EGRET objects. This resolution is important in addressing the question of source contribution to the flux and spectral slope of

the isotropic, presumably extragalactic gamma-ray background. Our results on these sources are discussed below (see Tables 3 and 4).

The source 2EG J1136−04 is a weak detection (shows extended emission) in the phase I + II data (only $\sim 4\ \sigma$ and only 36 counts above 100 MeV). A search for counterparts indicate the presence of two radio sources (1133−0413 and 1138−0350), both of which fall well below the limiting radio flux threshold value of 0.3 Jy.

The source 2EG J1233−14 is also detected at the 4 σ level, and the large error circle ($\sim 1\overset{\circ}{.}5$) shows no known radio source above our threshold. The 17 objects listed by NED are all either *IRAS* sources or galaxy clusters, neither of which is considered a likely gamma-ray source, given the EGRET sensitivity.

The position of 2EG J1239+04 is not well determined from the EGRET data that we have used here. Being close to 3C 273, the analysis does not yield well-defined position contours. Using the current position and error circle given in Table 3, a search yielded two potential candidates: 1237+0459 ($\alpha = 0.4$; flux at 4.85 GHz = 375 mJy) and PKS J1239+0519 ($\alpha = -0.66$; flux at 4.85 GHz = 340 mJy). Because of the lack of a well-defined source position, we do not consider these as likely identifications but rather as potential candidates that should be re-examined with additional phase III observations.

The source 2EG J1346+29 was detected primarily in VP 4. No strong radio source is known within the 56′ error circle. The two supernovae 1989W and 1990D are located within the error box. Since this is a high-latitude source, EGRET is more sensitive to emission from weak sources such as supernova remnants (SNRs). Various studies indicate SNRs could be gamma-ray sources (Drury, Aharonian, & Völk 1994; Esposito et al. 1996), and so there is some room for considering these as likely counterparts. However, if the time variability of this source can be established (phase I and II data are inadequate), then SNRs appear to be less likely, since, in general, the high-energy gamma-ray flux from an SNR is not expected to vary over timescales as short as a year.

Thus four of the sources in the region of study remain unidentified at present. Continued observations are expected to reduce the size of the error box, as well as provide a basis to study variations in intensity and spectrum.

5. OTHER INTERESTING SOURCES NOT SEEN BY EGRET

We discuss here observational results on a few interesting sources in our region of study that are not detected in the phase I + II data. These include the nearby galaxies M82 and M87, and the rich Coma Cluster of galaxies.

5.1. *M82*

M82 is one of the closest starburst galaxies, at a distance of 3.3 Mpc and characterized by an unusually high star formation rate. Massive star formation produces strong stellar winds and an enhanced supernova rate. This leads to the heating of the interstellar medium and the production of a lot of cosmic rays. The strong radio synchrotron emission indicates the mean energy density for relativistic electrons in the central region of M82 to be ≈ 60 eV cm^{-3}. Völk, Klein, & Wielebinski (1989) gave an estimate of 80 eV cm^{-3}. This is more than 3 orders of magnitude larger than the value determined in our local Galactic neighborhood (6000–8000 times larger, if local cosmic-ray electron density is taken to be 0.01 eV cm^{-3}). Assuming the standard value of the proton to electron ratio of 100, the significantly larger average cosmic-ray energy density implies enhanced gamma-ray production in the central region via nucleon-nucleon interaction and the electron bremsstrahlung processes. Sreekumar et al. (1994) has summarized the results from the early EGRET observations on M82. This analysis yields a 2 σ upper limit of 5×10^{-8} photons cm^{-2} s^{-1}.

5.2. *M87*

M87 is the largest nearby galaxy and the nearest giant elliptical (13 Mpc). Well known as the strong radio source Virgo A, M87 has a radio luminosity 1000 times greater than the Milky Way and has been extensively studied at many wavelengths. Being the largest and brightest elliptical galaxy in the Virgo Cluster, M87, which is located near the cluster's center, is thought to play an important role in its dynamics. Optical images show over 500 globular clusters around the galaxy and also a well-defined optical and radio jet emerging from the central region, maybe as close as 1.5 kpc from the central nucleus. Recent data from the *Hubble Space Telescope* (Harms et al. 1994) point to the presence of a supermassive black hole ($M > 10^9\ M_0$) at the center of M87. Gamma-ray observations can be used to study the presence of high-energy particles in the vicinity of such a supermassive blackhole. Previous efforts to examine the high-energy emission from M87 using the *SAS* 2 and *COS B* satellites provided only upper limits—1.0×10^{-6} photons cm^{-2} s^{-1} from *SAS 2* above 100 MeV (Fichtel et al. 1975) and an upper limit equivalent to 3×10^{-7} above 100 MeV from *COS B* (Pollock et al. 1981). We derive a 2 σ upper limit (95% confidence) of 4×10^{-8} photons cm^{-2} s^{-1} for $E \geq 100$ MeV, consistent with previous estimates of Sreekumar et al. (1994).

5.3. *Coma Cluster*

The Coma Cluster of galaxies is the closest (113 Mpc) rich cluster and most well studied galaxy cluster. It belongs to the richness class 2 and has a cluster diameter of about 160′. One of the interesting questions that can be addressed using gamma-ray observations is the role of cosmic rays in heating the intracluster medium. Early radio observations by Large, Mathewson, & Haslam (1961) showed a diffuse, steep spectrum radio halo. Coma appears to have the strongest radio halo among those clusters that sustain such an extended radio emission. It is believed that syncrotron emission from relativistic electrons in an intracluster magnetic field gives rise to this radio emission. Currently, the origin of these energetic electrons is still not understood. One possible scenario is that the halo emission arises from electrons that leak out of active radio galaxies however, the spatial extent of the halo is not consistent with a diffusion model (Jaffe 1977). Another possibility assumes that Coma-type radio halos are powered by secondary electrons generated by cosmic-ray protons interacting with the thermal ions in the intracluster medium (Dennison 1980; Vestrand 1980, 1994). X-ray observations indicate that the intergalactic medium in such clusters is filled wth thin, hot gas. Numerous studies (Lea & Holman 1978; Tucker & Rosner 1983) have addressed the possible reheating of the intracluster medium by cosmic rays streaming out of the galaxies. Böhringer & Morfill (1988) estimate that an energy input of $\sim 10^{44}$ ergs s^{-1} is required from cosmic rays to balance the

cooling of the intracluster gas. Clearly, both of the models discussed above require the presence of energetic cosmic rays in the cluster. These cosmic rays could give rise to gamma-ray emission because of their interaction with hot gas in the cluster. Assuming no proton contribution, Vestrand (1994) calculated the gamma-ray flux from electron bremsstrahlung to be

$$F(E_\gamma) = 7.5 \times 10^{-11} B^{-2.3} (E_\gamma/100\ \mathrm{MeV})^{-3.6}\ \mathrm{cm}^{-2}\ \mathrm{s}^{-1}\ \mathrm{MeV}^{-1}\ .$$

Assuming a range of field strength $B = 0.1$–$1.0\ \mu$G, the predicted flux above 100 MeV lies in the corresponding range 7.5×10^{-7}–3×10^{-9} photons cm^{-2} s^{-1}. EGRET observations during phases I and II of the Coma Cluster showed no detectable flux, and the derived 2 σ upper limit is 4×10^{-8} photons cm^{-2} s^{-1} for $E \geq 100$ MeV, which is significantly lower than that reported by McGlynn, Vestrand, & Jennings (1993) ($< 1.3 \times 10^{-7}$ photons cm^{-2} s^{-1}). Our upper limit to the gamma-ray flux from Coma translates to a minimum intracluster magnetic field strength of 0.4 μG. The minimum field strength would be even larger if there is also a finite contribution from cosmic-ray protons; however, there is no simple method for determining such a contribution. This estimate is 4 times larger than the minimum field of 0.1 μG obtained by Rephaeli, Ulmer, & Gruber (1994) from the OSSE data utilizing the absence of a hard Compton X-ray component.

6. CONCLUSION

A detailed analysis of EGRET observations of the north Galactic pole region ($b > 40°$) showed the presence of 15 strongly detected sources and six sources at the marginal 4 σ detection level. Of the total 21 sources, 17 have been identified primarily based on positional coincidence with the blazar class of AGNs. Sources such as 3C 279, PKS 1406−076, 1156+295, and 1222+216 show rapid variability in gamma rays, while others, such as Mrk 421 and 0917+449, appear to remain steady over the ~2.5 years covered by the phase I + II observations. Since EGRET observations are randomly spaced in time, this may not represent the true nature of these seemingly steady sources. The limited correlative multiwavelength data that is available at present shows no strong correlation between gamma-ray emission and emission at other wavelengths. This will have to be an important goal of future observations, since it may be the only way toward constraining AGN models.

EGRET observations have also yielded other gamma-ray point sources that have not yet been identified with source candidates at other wavelengths. A subset of these show time variability and hence cannot be classified as being due to underestimation of the constant Galactic background. Additional observations on the steady sources will provide significantly smaller error circles to search for counterparts. It is important to address the identification of these sources, since the class of objects they may represent, such as weaker radio sources or a new class of gamma-ray bright objects, could contribute significantly to the observed extragalactic gamma-ray emission.

The authors wish to thank an anonymous referee for helpful comments and suggestions that resulted in a more concise manuscript. They also thank Laura McDonald for assistance with the figures. The EGRET team gratefully acknowledges support from the following: Bundesministerium für Forschung und Technologie grant 50 QV 9065 (MPE), NASA Grant NAG5-1742 (HSC), NASA Grant NAG5-1605 (SU), and NASA Contract NAS5-31210 (GAC). This research has made use of the NASA/IPAC Extragalactic Database (NED), which is operated by the Jet Propulsion Laboratory, California Institute of Technology, under contract with the National Aeronautics and Space Administration, and of the Simbad database, operated at CDS, Strasbourg, France. This research has also made use of NASA's Astrophysics Data System, Astrophysics Science Information, and Abstract Service.

REFERENCES

Agarwal, P. C., Singh, K. P., & Riegler, G. R. 1987, MNRAS, 227, 525
Bertsch, D. L., et al. 1996, in preparation
Bertsch, D. L., Dame, T. M., Fichtel, C. E., Hunter, S. D., Sreekumar, P., Stacy, J. G., & Thaddeus, P. 1993, ApJ, 416, 587
Bignami, G. F., et al. 1981, A&A, 93, 71
Blandford, R. D., & Königl, A. 1979, ApJ, 232, 34
Blandford, R. D., & Rees, M. J. 1978, in Pittsburgh Conference on BL Lac Objects, ed. A. N. Wolfe (Pittsburgh: Univ. Pittsburgh Press), 328
Bloom, S. D., & Marscher, A. P. 1992, in Compton Observatory Science Workshop, NASA Conf. Publ. 313, ed. C. R. Shrader, N. Gehrels, & B. Dennis (Washington: NASA), 339
Böhringer, H., & Morfill, G. E. 1988, ApJ, 330, 609
Courvoisier, T. J.-L., et al. 1987, A&A, 176, 197
Dennison, B. 1980, ApJ, 236, 761
Dermer, C. D., Schlickeiser, R., & Mastichiadis, A. 1992, in Compton Observatory Science Workshop, NASA Conf. Publ. 3137, ed. C. R. Shrader, N. Gehrels, & B. Dennis (Washington: NASA), 328
Dingus, B. L., et al. 1993, IAU Circ. 5680
———. 1996, ApJ, in press
Drury, L. O'C., Aharonian, F. A., & Völk, H. J. 1994, A&A, 287, 959
Esposito, J. A., Hunter, S. D., Kanbach, G., & Sreekumar, P. 1996, ApJ, 461, 820
Fichtel, C. E., et al. 1975, ApJ, 198, 163
———. 1994, ApJS, 94, 551
Ginzburg, V., & Syrovatski, S. I. 1969, ARA&A, 7, 375
Harms, R. J., et al. 1994, ApJ, 435, L35
Hartman, R. C., et al. 1992, ApJ, 385, L1
———. 1993, in AIP Conf. Proc. 304, The Second Compton Symp., ed. C. Fichtel, N. Gehrels, & J. Norris (New York: AIP), 563
Hermsen, W., et al. 1981, Proc. 17th Int. Cosmic-Ray Conf. (Paris), 1, 230
Hunter, S. D., et al. 1996, ApJ, , submitted
Impey, C. D., & Tapia, S. 1990, ApJ, 354, 124
Jaffe, W. J. 1977, ApJ, 212, 1
Kanbach, G., et al. 1996, in preparation
———. 1988, Space Sci. Rev., 49, 69
Kerrick, A. D. 1994, IAU Circ., 5996
Kerrick, A. D., et al. 1995, ApJ, 438, L59
Kniffen, D. A., et al. 1993, ApJ, 411, 133
———. 1996, ApJ, in press
Large, M. I., Mathewson, D. S., & Haslam, C. G. T. 1961, MNRAS, 123, 113
Lea, S. M., & Holman, G. D. 1978, ApJ, 222, 29
Lin, Y. C., et al. 1992, ApJ, 401, L61
———. 1993, in AIP Conf. Proc. 304, The Second Compton Symp., ed. C. Fichtel, N. Gehrels, & J. Norris (New York: AIP), 582
———. 1996, ApJ, accepted
Maraschi, L., Ghisellini, G., & Celotti, A. 1992, ApJ, 397, L5
Massaro, E., Nesci, R., & Perola, G. C. 1992, IAU Circ., 5458
Mattox, J. R., et al. 1993, ApJ, 410, 609
———. 1996a, in preparation
———. 1996b, ApJ, 461, 396
McGlynn, T. A., Vestrand, W. T., & Jennings, D. 1993, in AIP Conf. Proc. 304, The Second Compton Symp., ed. C. Fichtel, N. Gehrels, & J. Norris (New York: AIP), 669
Melia, F., & Königl, A. 1989, ApJ, 340, 162
Mohanty, G., et al. 1993, Proc. 23rd Int. Cosmic Ray Conf. (Calgary), 1, 440
Mukherjee, R., et al. 1995, ApJ, 445, 189
———. 1996, ApJ, submitted
Nolan, P. L., et al. 1996, ApJ, 459, 100
Pollock, A. M. T., et al. 1981, A&A, 94, 116
Punch, M., et al. 1992, Nature, 358, 477

Rephaeli, Y., Ulmer, M., & Gruber, D. 1994, ApJ, 429, 554
Sambruna, R. M., Barr, P., Giommi, P., Maraschi, L., Tagliaferri, G., & Treves, A. 1994, ApJ, 434, 468
Schubnell, M., et al. 1993, in AIP Conf. Proc. 304, The Second Compton Symp., ed. C. Fichtel, N. Gehrels, & J. Norris (New York: AIP), 597
Sikora, M., Begelman, J. G., & Rees, M. J. 1994, ApJ, 421, 153
Sreekumar, P., et al. 1992, ApJ, 400, L67
———. 1994, ApJ, 426, 105
Sreekumar, P., & Kniffen, D. A. 1996, in IAU Symp. 168, Examining the Big Bang and Diffuse Background Radiation, ed. M. Kafatos & Y. Kondo (The Hague: Kluwer), 279
Sreekumar, P., et al. 1996, in preparation
Swanenburg, B. N., et al. 1978, Nature, 275, 298
Takahashi, T., et al. 1994, IAU Circ. 5993
Thompson, D. J., & Fichtel, C. E. 1982, A&A, 109, 352
Thompson, D. J., et al. 1993a, ApJS, 86, 629
———. 1993b, ApJ, 415, L13
———. 1995, ApJS, 101, 259
Tucker, W. H., & Rosner, R. 1983, ApJ, 267, 547
Ulrich, M. H., Courvoisier, T. J.-L., & Wamsteker, W. 1993, ApJ, 411, 125
Vestrand, W. T. 1980, Ph.D. thesis, Univ. Maryland, College Park
———. 1994, unpublished work
Völk, H. J., Klein, U., & Wielebinski, R. 1989, A&A, 213, L12
von Montigny, C., et al. 1993, A&AS, 97, 101
———. 1995, ApJ, 440, 525